COMPDYN 2017
6th ECCOMAS Thematic Conference on
Computational Methods in Structural Dynamics and Earthquake Engineering
M. Papadrakakis, M. Fragiadakis (eds.)
Rhodes Island, Greece, 15–17 June 2017

QUASI-KINEMATIC RESPONSE OF EMBEDDED FOUNDATIONS: EVIDENCE OF FOUNDATION MASS EFFECT FROM NUMERICAL ANALYSES AND INSTRUMENTED STRUCTURES

Riccardo Conti[1], Marco Morigi[2], Giulia Viggiani[2], Emmanouil Rovithis[3], Nikos Theodoulidis[3] and Christos Karakostas[3]

[1] Università di Roma Niccolò Cusano
Via Don Carlo Gnocchi 3, 00166, Rome, Italy
riccardo.conti@unicusano.it

[2] Università di Roma Tor Vergata
Via del Politecnico 1, 00133, Rome, Italy
{viggiani,marco.morigi}@uniroma2.it

[3] Institute of Engineering Seismology and Earthquake Engineering, EPPO-ITSAK
Dasiliou Str., Eleones, Pylaia, 55535, Thessaloniki, Greece
{rovithis,ntheo,christos}@itsak.gr

Keywords: Massive foundations, kinematic interaction factors, numerical FDM analyses, earthquake recordings.

Abstract. *Experimental and theoretical studies on soil-structure interaction (SSI) have demonstrated that the seismic motion imposed at the foundation of a structure may be different from the free-field motion due to the filtering action exerted by the foundation. In the realm of the substructure approach, the above kinematic interaction effect is investigated by disregarding the foundation mass. However, in the case of massive foundations supporting high-rise and/or wide plan view buildings or large monumental structures, foundation mass may contribute to the final input motion. This paper investigates the role of the foundation mass on the filtering action of embedded foundations by means of FDM numerical analyses. New analytical expressions of quasi-kinematic interaction factors are proposed, allowing for a direct implementation in analysis or design of massive foundations. The role of salient model parameters, such as the soil-to-foundation mass density ratio, the dimensionless frequency of the input motion and the aspect ratio of the foundation, is explored. The proposed analytical model is then compared with earthquake recordings from two accelerometric stations, maintained by ITSAK, that are installed at the free-field and at the basement of a nearby instrumented building with a massive embedded foundation.*

1 INTRODUCTION

It is well known that the dynamic behavior of buildings can be affected by the presence of a deformable soil-foundation system, which possibly makes the seismic response of a flexibly-supported structure different from that of the rigidly-supported counterpart [1] by: (i) lengthening the fundamental period of the structure; (ii) allowing additional dissipation of energy into the soil by radiation and hysteresis; (iii) filtering the signal transmitted to the structure by incident waves, as a result of both base slab averaging [2] and embedment effects [3].

Following the concept of the substructure approach, the motion of the foundation as part of a coupled Soil-Structure Interaction (SSI) system is usually regarded as the contribution of two concurrent phenomena [4]: (i) kinematic interaction, in which a massless foundation modifies the motion of the surrounding soil depending on its stiffness and (ii) inertial interaction, in which the motion of the foundation itself is further modified by the inertia forces acting in the structure-foundation system.

By focusing on the filtering action of the foundation, kinematic interaction has been recognized to play a significant role in the case of both embedded [5] and deep foundations [6], where the foundation input motion (FIM) may differ substantially from the free-field motion at ground surface. Further studies, taking into account both the soil-foundation system and the superstructure, have shown that the filtering effect is usually beneficial for squat structures while it may be detrimental for slender buildings with deeply embedded foundations or basements [7] by increasing the ductility demand.

In the case of rigid embedded foundations, scattering effects reduce the horizontal displacement of the base slab, u_G, with respect to the free-field motion, u_{ff}, while introducing a rotational component, θ_G, with no counterpart in a fixed base structure. Under the assumptions of massless foundation and vertically propagating plane shear waves, the latter implying that base slab averaging cannot occur, filtering effect is physically related to the inability of the foundation elements to follow soil deformations induced by travelling waves, especially for short wavelengths. Further studies have also shown that the mass of the foundation can provide a significant contribution in filtering the free-field motion [8-11]. The overall phenomenon can be described by three kinematic response factors, namely $I_u = u_G/u_{ff}$, $I_{u,top} = u_A/u_{ff}$ and $I_\theta = \theta_G H/u_{ff}$, which are frequency-dependent transfer functions relating the harmonic steady-state motion experienced by the foundation to the amplitude of the corresponding free-field surface motion (Figure 1). Specifically, I_u and I_θ, referring to the base slab of the foundation, are the standard kinematic factors used in the case of massless foundation [12], while $I_{u,top}$ refers to the top of a massive foundation.

A series of studies in the literature explore the problem of filtering effects induced by rigid embedded foundations, using different numerical techniques. However, most of them refer to the case of a massless rigid foundation – with cylindrical or rectangular shape - embedded in a uniform elastic or viscoelastic half-space [13-17]. Going to the seismic design practice, the filtering effect induced by embedded massless foundations is usually described using the simplified formulas proposed by Elsabee & Morray [3] approximating rigorous FE analyses, essentially relating the motion of the rigid foundation to the translation of the free-field at the foundation level. An improved version of the above formulas has been recently proposed by Conti *et al*. [12], based on the best fit of numerical FDM results.

This paper presents a numerical and theoretical study of the filtering effect induced by rigid massive embedded foundations. The goal of this work is: (i) to extend the observations already available in the literature for the case of a massless foundation and (ii) to define new simplified, but physically sound solutions to be incorporated in recommendations for the seismic design of structures with embedded foundations. To validate the numerical results, the

proposed solutions are compared with earthquake recordings from two accelerometric stations installed at the free-field and the basement of an instrumented building with a massive embedded foundation.

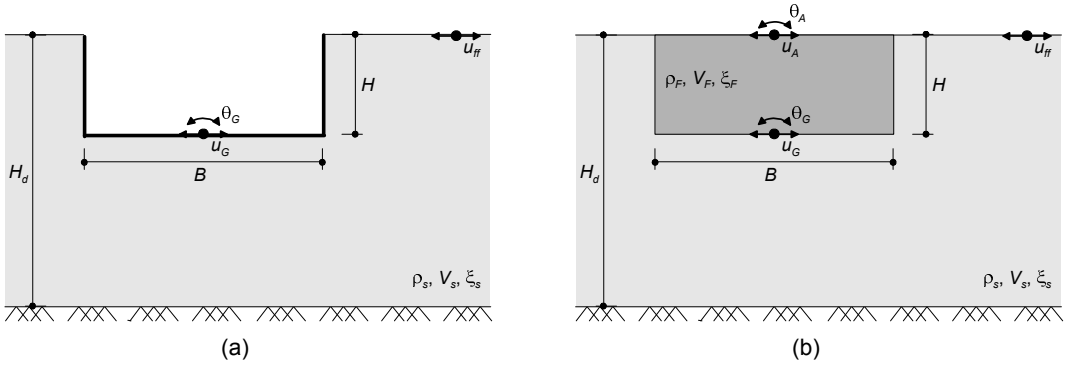

Figure 1: Problem layout and relevant parameters for: (a) massless and (b) massive embedded foundations.

2 PROBLEM DEFINITION AND DIMENSIONAL ANALYSIS

Under the assumption of vertically propagating plane shear waves, the dimensionless groups governing the filtering effect induced by embedded foundations can be derived. We refer to the general case of a rigid rectangular foundation (embedment depth H, width B, length L, mass density ρ_F, shear modulus G_F, damping ratio ξ_F) embedded in a homogeneous isotropic visco-elastic soil layer (thickness H_d, mass density ρ_S, shear modulus G_S, Poisson's ratio ν_S, damping ratio ξ_S). Given for simplicity $\xi_F = \xi_S = \xi$ and assuming $\theta_A = \theta_G$, which strictly holds for rigid foundations, the problem can be formulated as:

$$\begin{aligned} u_G &= f\left(u_{ff}, \omega, H, B, L, \rho_F, G_F, \rho_S, G_S, \xi, \nu_S, H_d\right) \\ \theta_G &= g\left(u_{ff}, \omega, H, B, L, \rho_F, G_F, \rho_S, G_S, \xi, \nu_S, H_d\right) \\ u_A &= s\left(u_{ff}, \omega, H, B, L, \rho_F, G_F, \rho_S, G_S, \xi, \nu_S, H_d\right) \end{aligned} \tag{1}$$

Applying the Buckingham theorem, it is possible to rescale Equations (1) in dimensionless form, using H, G_S and ρ_S as dimensionally independent variables:

$$\begin{aligned} I_u &:= \frac{u_G}{u_{ff}} = F\left(\frac{\omega H}{V_S}, \frac{\rho_F}{\rho_S}, \frac{G_F}{G_S}, \frac{B}{H}, \frac{L}{H}, \frac{H_d}{H}, \xi, \nu_S\right) \\ I_\theta &:= \frac{\theta_G H}{u_{ff}} = G\left(\frac{\omega H}{V_S}, \frac{\rho_F}{\rho_S}, \frac{G_F}{G_S}, \frac{B}{H}, \frac{L}{H}, \frac{H_d}{H}, \xi, \nu_S\right) \\ I_{u,top} &:= \frac{u_A}{u_{ff}} = S\left(\frac{\omega H}{V_S}, \frac{\rho_F}{\rho_S}, \frac{G_F}{G_S}, \frac{B}{H}, \frac{L}{H}, \frac{H_d}{H}, \xi, \nu_S\right) \end{aligned} \tag{2}$$

In order to reduce the dimensionless parameters involved, some simplifying assumptions are usually introduced in the literature, *i.e.*: the embedded foundation is rigid ($G_F/G_S \gg 1$) and the soil deposit is assimilated to a homogeneous half-space ($H_d/H \gg 1$). With reference to ξ and ν_S, numerical investigations have shown that, while these parameters affect the dynamic response of both the foundation and the soil, they have a minor influence on the kinematic response factors [6,17]. Moreover, Conti *et al.* [12] have shown that only the foundation width B in the polarization plane of the shear wave affects the filtering phenomenon, denoting that the aspect ratio (L/H) of the foundation may be disregarded. Under these assumptions, the interaction factors can be expressed as functions of three sole parameters:

$$I_u := \frac{u_G}{u_{ff}} = F\left(\frac{\omega H}{V_S}, \frac{\rho_F}{\rho_S}, \frac{B}{H}\right)$$
$$I_\theta := \frac{\theta_G H}{u_{ff}} = G\left(\frac{\omega H}{V_S}, \frac{\rho_F}{\rho_S}, \frac{B}{H}\right) \quad (3)$$
$$I_{u,top} := \frac{u_A}{u_{ff}} = S\left(\frac{\omega H}{V_S}, \frac{\rho_F}{\rho_S}, \frac{B}{H}\right)$$

The dimensionless ratios in Equation (3) take into account the physical, mechanical and geometrical properties of the problem at hand. Specifically, $\omega H/V_S$ refers to the ratio of the embedment depth of the foundation over the wavelength of the excitation, which practically means that larger wavelengths may be filtered by scattering effects with increasing embedment depth. On the other hand, ρ_F/ρ_S is the mass density ratio between the foundation and the soil, indicating stronger filtering action with increasing mass density of the foundation.

3 NUMERICAL STUDY

Plane-strain analyses of a rectangular massive foundation of width B, embedment depth H and mass density ρ_F, embedded in an homogeneous half-space, were carried out in time domain using the finite difference code FLAC 2D v7 [18], with the ratios B/H and ρ_F/ρ_S ranging from 0.25 to 6 and from 0 to 1.3 respectively. A detailed description of the numerical models is reported in Conti *et al*. [12].

3.1 Model description

Both the soil and the massive foundation were modelled as linear visco-elastic isotropic materials (mass density ρ_S = 1.835 t/m^3; shear wave velocities V_S = 100 m/s and $V_F = 10V_S$; Poisson ratios $\nu_S = \nu_F = 0.3$). A stiffness ratio of $G_F/G_S = 100$ was assumed in order to guarantee the assumption of rigid foundation, while four different values were considered for the mass density ratio ρ_F/ρ_S at 0, 0.5, 1.0 and 1.3. A Rayleigh viscous damping was used, with a given value of 2 % at the reference frequencies of 1 Hz and 10 Hz.

Free-field boundary conditions were applied along the lateral sides of the mesh, involving the coupling of the main grid with a one-dimensional free-field column through viscous dashpots, in such a way that outward waves originating from the interior of the model can be properly absorbed. As far as the boundary condition at the base of the mesh is concerned, both viscous dashpots and the dynamic input were applied in order to reproduce the upward propagation of shear waves within a semi-infinite domain. The input was a constant amplitude sinusoidal sweep, defined in terms of a horizontal displacement time history, with a duration of 60 s and a frequency increasing linearly with time from 0.5 to 10 Hz. This range was chosen to include the typical frequency content of real earthquakes.

The rigid rotation of the foundation was computed as $(v_R(t)\text{-}v_L(t))/B$, where $v_R(t)$ and $v_L(t)$ are the vertical displacements at the right and left corners of the foundation base, respectively. The free field motion, u_{ff}, was obtained from a one-dimensional analysis. As an example, Figure 2 shows: (a) the amplitude Fourier spectra of $u_G(t)$ and $u_{ff}(t)$ together with the absolute value of I_u, and; (b) the amplitude Fourier spectra of $\theta_G(t)$ and $u_{ff}(t)$ together with the absolute value of I_θ, obtained from one of the analyses performed.

3.2 Results

Numerical results are summarized in Figures 3, 4 and 5, showing the amplitude of I_u, I_θ and $I_{u,top}$, respectively. The interaction factors are given as a function of the dimensionless frequency $\omega H/V_S$, for different values of the aspect ratio B/H and of the density ratio ρ_F/ρ_S.

For small B/H (squat/slender foundations), the interaction factors are not significantly affected by the mass density ratio and all tend to the free-field 1D condition, where filtering effects are mostly due to the embedment of base slab [12]. In this condition, $|I_u|$ shows an oscillating trend, with local minima and maxima clearly related to the resonant frequencies of the corresponding free-field case, and a significant rocking component emerges in the foundation motion, as reflected by $|I_\theta|$, while $|I_{u,top}|$ tends to unity ($u_A = u_{ff}$).

A completely different behaviour is observed for large B/H values (spread foundations). In this case, the density ratio ρ_F/ρ_S affects both $|I_u|$ and $|I_{u,top}|$. For $\rho_F/\rho_S = 0$ (massless foundation) $|I_u|$ tends to one, which is the corresponding limit solution for $B/H = \infty$, while for $\rho_F/\rho_S \neq 0$ the kinematic factor moves towards other asymptotic solutions, depending on the mass density ratio. Concurrently, as reflected by the almost zero values of $|I_\theta|$, no significant rocking motion is mobilized and, therefore, $|I_u|$ and $|I_{u,top}|$ tend to coincide.

Based on the above observations, it can be concluded that all the kinematic factors are strongly affected by the aspect ratio of the foundation, B/H, and are not related merely to the embedment depth of the foundation. Moreover, the mass of the foundation can modify substantially the filtering action induced by a rigid embedded foundation, with respect to the massless case, especially in the case of large B/H ratios.

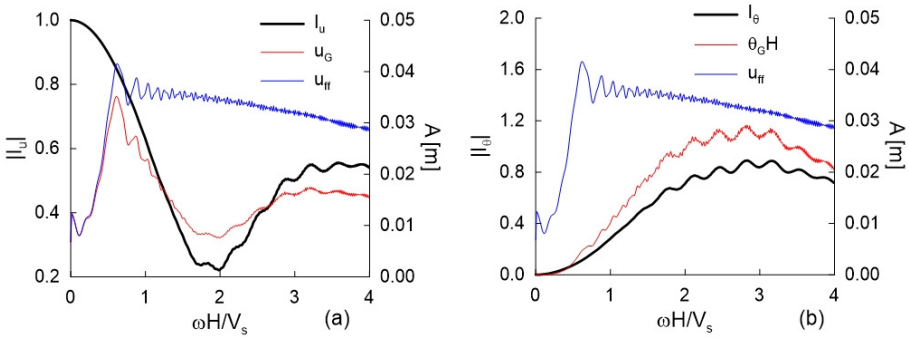

Figure 2: Numerical analyses. Kinematic interaction factors for $B/H = 1$ and $\rho_F/\rho_S = 1$: (a) $|I_u|$ and (b) $|I_\theta|$.

4 SIMPLIFIED THEORETICAL MODEL

Similarly to the approach followed in [12], two limit 1D cases can be identified for the problem at hand, referring to an infinitely thin ($B/H \to 0$) and an infinitely extended ($B/H \to \infty$) foundation, respectively.

4.1 Limit case for B/H=0 (infinitely narrow foundation)

For this specific limit case, the difference between the foundation motion and the free-field surface motion is only due to the variation of ground motion with depth. As a consequence, the three kinematic interaction factors do not depend on the mass density ratio and can be computed with reference to the free-field motion in the embedment region, assuming elastic behaviour for the soil ($\xi_s = 0$), as:

$$
\begin{aligned}
I_u|_{(B/H=0)} &= \frac{u_{ff}|_{z=H}}{u_{ff}} = \cos\left(\frac{\omega H}{V_S}\right) \\
I_\theta|_{(B/H=0)} &= \frac{\theta_{ff} \cdot H}{u_{ff}} = 1 - \cos\left(\frac{\omega H}{V_S}\right) \\
I_{u,top}|_{(B/H=0)} &= \frac{u_{ff}|_{z=0}}{u_{ff}} = 1
\end{aligned}
\tag{4}
$$

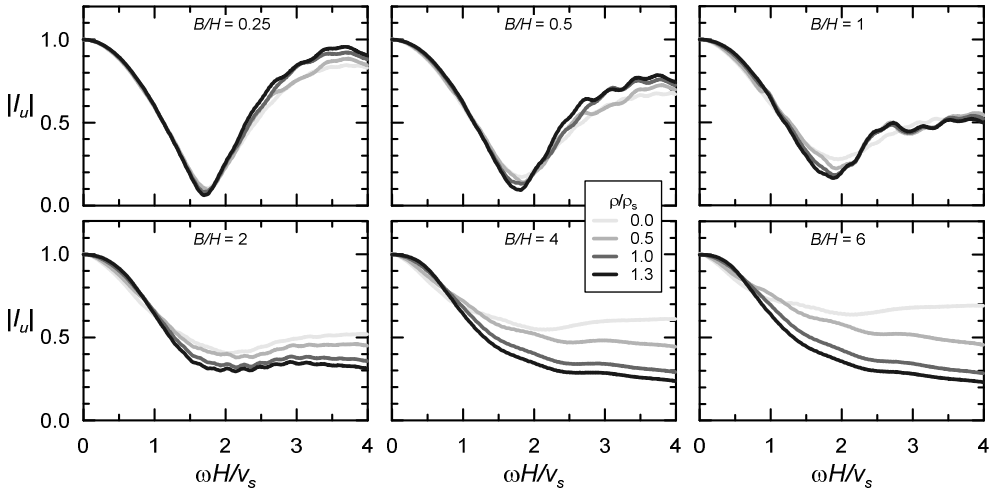

Figure 3: Numerical analyses. Absolute value of I_u computed for different values of B/H and ρ_F/ρ_S.

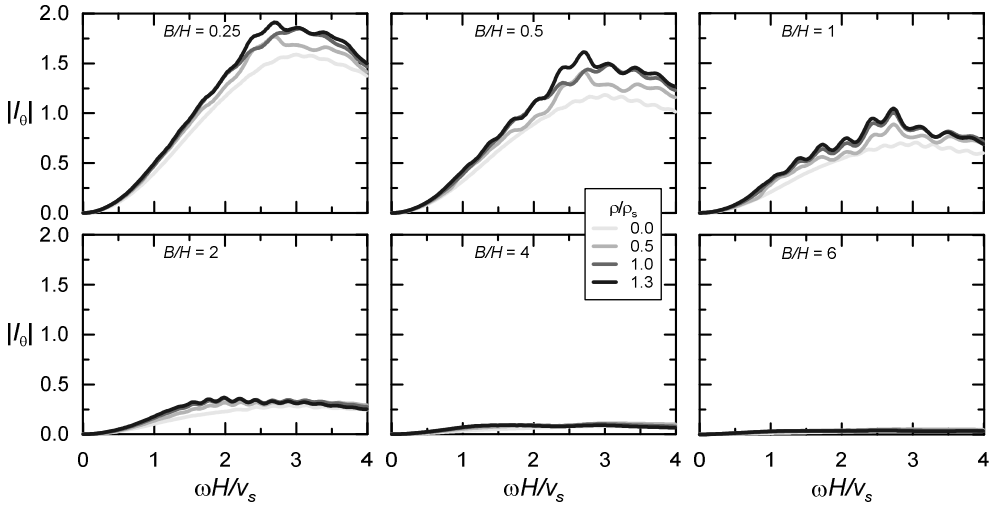

Figure 4: Numerical analyses. Absolute value of I_θ computed for different values of B/H and ρ_F/ρ_S.

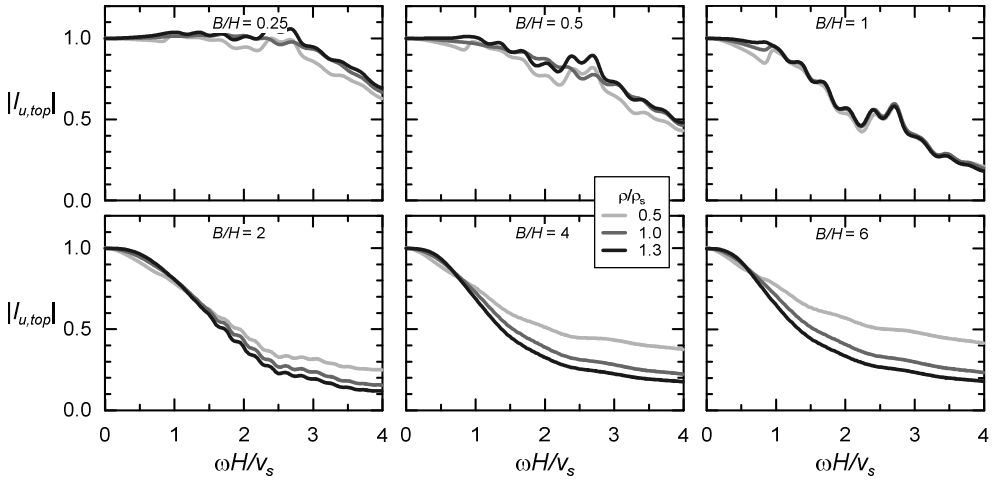

Figure 5: Numerical analyses. Absolute value of $I_{u,top}$ computed for different values of B/H and ρ_F/ρ_S.

4.2 Limit case for $B/H=\infty$ (infinitely extended foundation)

Upon implementing the reference system of Figure 6(b, c), we can define:

$$\begin{aligned} I_u &:= \frac{u_G}{u_{ff}} = \frac{u_G}{u_{bed}}\frac{u_{bed}}{u_{ff}} \\ I_{u,top} &:= \frac{u_A}{u_{ff}} = \frac{u_A}{u_{bed}}\frac{u_{bed}}{u_{ff}} = \frac{u_A}{u_G}\frac{u_G}{u_{bed}}\frac{u_{bed}}{u_{ff}} = \frac{u_A}{u_G}I_u \end{aligned} \tag{5}$$

where, from a standard response analysis of a viscoelastic soil layer one gets:

$$\begin{aligned} \frac{u_{ff}}{u_{bed}} &= \frac{1}{\cos k_S^* H_d} \\ \frac{u_A}{u_G} &= \frac{1}{\cos k_F^* H} \end{aligned} \tag{6}$$

The wave numbers k_S^* (soil) and k_F^* (foundation) are given by the expressions:

$$k_S^* = \frac{\omega}{V_S^*}, \quad k_F^* = \frac{\omega}{V_F^*} \tag{7}$$

where:

$$V_S^* = V_S(1 + i\xi_S), \quad V_F^* = V_F(1 + i\xi_F) \tag{8}$$

are the complex shear wave velocities of the soil and of the foundation respectively. The dynamic response of the 2-layer system of Figure 6(b) yields:

$$\begin{aligned} I_u &= \frac{\cos k_S^* H_d \cos k_F^* H}{\cos k_S^*(H_d - H)\cos k_F^* H - \alpha^* \sin k_S^*(H_d - H)\sin k_F^* H} \\ I_{u,top} &= \frac{\cos k_S^* H_d}{\cos k_S^*(H_d - H)\cos k_F^* H - \alpha^* \sin k_S^*(H_d - H)\sin k_F^* H} \end{aligned} \tag{9}$$

where α^* is the complex impedance ratio, given by:

$$\alpha^* = \frac{\rho_F V_F^*}{\rho_S V_S^*} \tag{10}$$

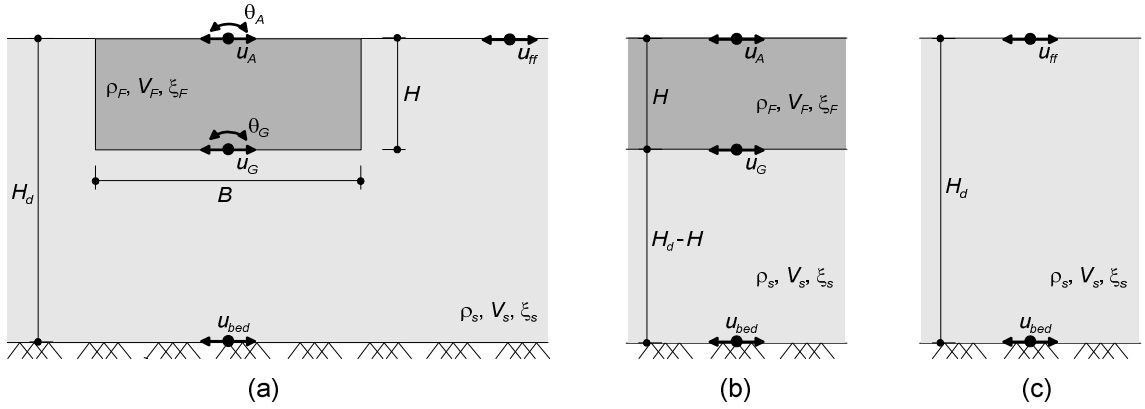

Figure 6: Massive embedded foundations. (a) 2D problem layout; (b) 1D theoretical model of a 2-layer system corresponding to an infinitely extended foundation and (c) free-field homogeneous layer.

After some manipulation, it is possible to derive simplified expressions of the absolute values of I_u and $I_{u,top}$ for the half-space condition ($H_d/H \gg 1$) and for an infinitely rigid foundation ($V_F/V_S \gg 1$). Specifically, upon assuming that $\xi_S \ll 1$ and $\xi_F \ll 1$ and for bounded values of ω (which is reasonable for real earthquakes), we can write:

$$|I_u|_{\substack{H_d\to\infty \\ V_F\to\infty}} = \left|I_{u,top}\right|_{\substack{H_d\to\infty \\ V_F\to\infty}} = \frac{1}{\sqrt{1+\left(\frac{\rho_F}{\rho_S}\right)^2\left(\frac{\omega H}{V_S}\right)^2}} \tag{11}$$

4.3 2D simplified solutions

Simplified expressions for $|I_u|$, $|I_\theta|$ and $|I_{u,top}|$, suitable for taking into account kinematic effects in design and/or analysis of massive embedded foundations can be defined using *ad hoc* functions which allow to recover the two 1D limit cases mentioned above for $B/H\to 0$ and $B/H\to\infty$. Specifically, based on numerical results and bearing in mind the two 1D limit solutions, the following functions for $|I_u|$, $|I_\theta|$ and $|I_{u,top}|$ are proposed:

$$\begin{aligned}
\left|I_u\left(\frac{B}{H},\frac{\rho_F}{\rho_S},\frac{\omega H}{V_S}\right)\right| &= \frac{a_1}{\sqrt{1+\left(\frac{\rho_F}{\rho_S}\frac{\omega H}{V_S}\right)^2}} + \frac{(1-a_1)}{\left[1+\left(\frac{\omega H}{V_S}\right)^2\right]^{a_1 a_3}}\cdot\left|\cos\left(a_2\frac{\omega H}{V_S}\right)\right| \\
\left|I_\theta\left(\frac{B}{H},\frac{\omega H}{V_S}\right)\right| &= a_5\cdot\left|1-\cos\left(\frac{\omega H}{V_S}\right)\right| \\
\left|I_{u,top}\left(\frac{B}{H},\frac{\rho_F}{\rho_S},\frac{\omega H}{V_S}\right)\right| &= \frac{1}{\sqrt{1+a_4{}^2\left(\frac{\rho_F}{\rho_S}\frac{\omega H}{V_S}\right)^2}}
\end{aligned} \tag{12}$$

where the coefficients a_1, a_3, governing $|I_u|$, depend on the ratios B/H and ρ_F/ρ_s, while the coefficients a_2, a_4, a_5 are a function of the ratio B/H, as presented in the following:

$$\begin{aligned}
&a_1\left(\frac{B}{H},\frac{\rho_F}{\rho_S}\right) = \frac{(B/H)^\alpha}{\beta+(B/H)^\alpha} && \alpha = 1.0+0.6\left(\frac{\rho_F}{\rho_S}\right) && \beta = 3.3-1.4\left(\frac{\rho_F}{\rho_S}\right) \\
&a_2\left(\frac{B}{H}\right) = \frac{1+\alpha(B/H)}{1+(B/H)} && \alpha = 0.7 && \\
&a_3\left(\frac{\rho_F}{\rho_S}\right) = 2.2-1.6\left(\frac{\rho_F}{\rho_S}\right) && && \\
&a_4\left(\frac{B}{H}\right) = \frac{(B/H)^\alpha}{\beta+(B/H)^\alpha} && \alpha = 2.0 && \beta = 0.5 \\
&a_5\left(\frac{B}{H}\right) = \frac{1}{1+\alpha(B/H)^\beta} && \alpha = 1.2 && \beta = 1.8
\end{aligned} \tag{13}$$

Figures 7, 8 and 9 compare numerical results, in terms of $|I_u|$, $|I_\theta|$ and $|I_{u,top}|$, with the theoretical Equations (12). Both the 1D solutions and the 2D approximate functions provide a good description of the actual trend exhibited by the kinematic interaction factors, in the whole frequency range of $0<\omega H/V_S<4$, which is typical of real earthquakes. As far as $|I_u|$ is concerned (Figure 7), for mass ratios above unity ($\rho_F/\rho_S>1$) and frequencies up to the fundamental frequency of the soil deposit (where $|I_u|$ tends to zero), the effect of the mass ratio is dominant over the B/H parameter. As a matter of fact, all the curves almost converge to a single one for the mass ratio $\rho_F/\rho_S = 1.3$. Going to $|I_{u,top}|$ (Figure 9), for $\rho_F/\rho_S=0.5$ the numerical results do not exhibit a monotonic trend towards the 1D limit solution for $B/H\to\infty$, which, nonetheless, seems to provide the right asymptotic value for the problem at hand.

5 COMPARISON WITH EARTHQUAKE RECORDINGS

5.1 COSMOS Offices building in Thessaloniki

The Cosmos Offices building complex, which hosted the premises of the Institute of Engineering Seismology and Earthquake Engineering (ITSAK) in Thessaloniki, is composed of four identical three-storey reinforced concrete buildings (No.1-4 in Figure 10) with basement.

The four buildings are separated by seismic joints and can thus be considered as statically independent in terms of seismic response. Moment resisting frames constitute the main load-resisting system of the structure. Each building has plan dimensions of 29.4 m x 33 m along the longitudinal (x-x) and the transverse (y-y) direction of the building complex, respectively, while its aboveground height is 10.6 m.

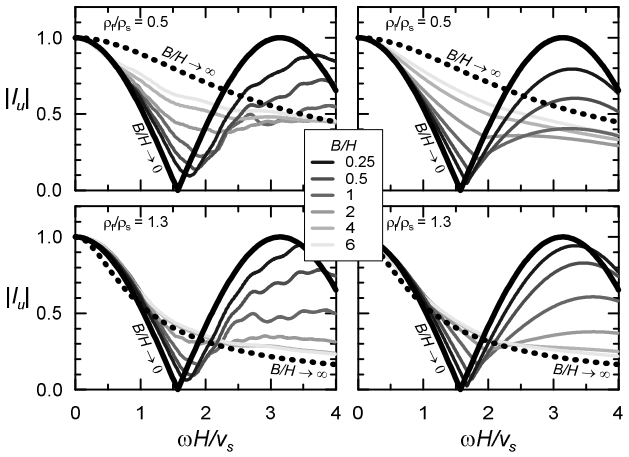

Figure 7: Amplitude of I_u. Comparison between numerical (left) and theoretical (right) results.

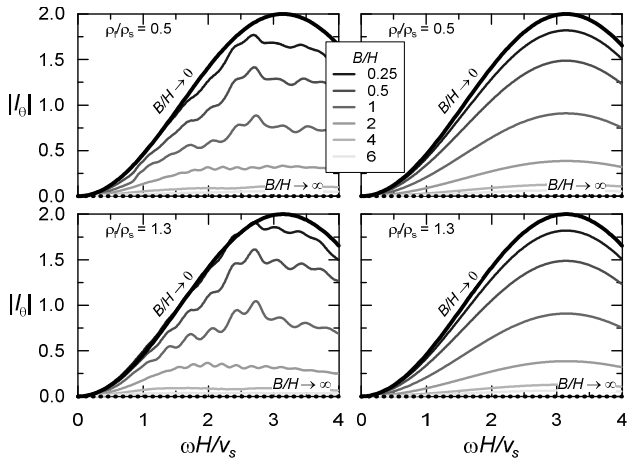

Figure 8: Amplitude of I_θ. Comparison between numerical (left) and theoretical (right) results.

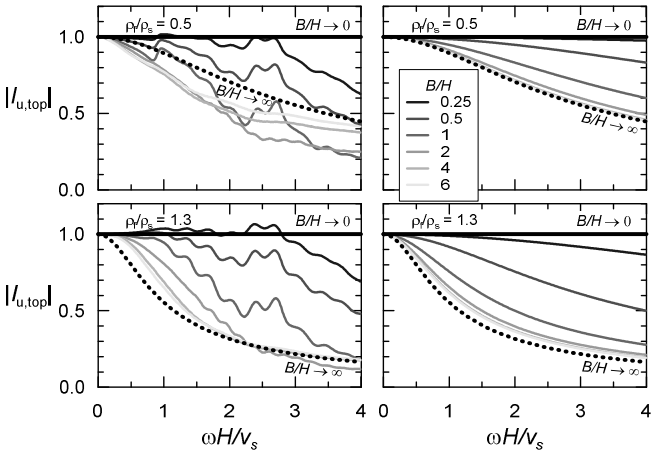

Figure 9: Amplitude of $I_{u,top}$. Comparison between numerical (left) and theoretical (right) results.

The basement of the building complex has shear walls 0.30 m thick along its perimeter. The foundation, at a depth of 4.8 m, is composed of interconnected grid beams. A typical plan view of the foundation, referring to building No.2 (which houses the accelerometric station T5u66 at its basement), is shown in Fig. 11(a). The exact dimensions of the structural configuration were retrieved from the design study of the building.

Upon evaluating the actual mass and stiffness of the structure, a simple MDOF lumped mass model was developed to estimate the first-mode period of building No.2 under fixed-base conditions. The modal analysis - performed by the FE code SAP2000 [19] - yielded a fundamental eigenperiod of the structure of $T_{x\text{-}x} = 0.47$ s and $T_{y\text{-}y} = 0.40$ s, along the x-x and y-y direction respectively, both activating approximately 76% of the total mass.

With reference to the geotechnical characterization of the soil deposit, a series of microtremor array field measurements were performed by Manakou *et al*. [20] at a distance of approximately 600 m away from the COSMOS site. The analysis of microtremor data revealed a piecewise increase of shear wave propagation velocity (V_S) from 160 m/sec at the ground surface to 460 m/sec at the depth of 30 m (Fig. 11(b)). The former value of V_S was adopted during the interpretation of earthquake recordings reported in the following. Mass density of the foundation soil was considered equal to $\rho_S = 1.8$ t/m^3.

5.2 Instrumentation and available earthquake recordings

The instrumentation of COSMOS Offices comprises two Guralp CMG-5TD high-resolution (24bits) accelerometric stations with absolute GPS time (Fig. 10), as part of the Greek National Accelerometric Network operated and maintained by ITSAK. The first station (T5u66), referred hereafter as the "foundation" station, is mounted on the reinforced concrete slab of the building's basement while the second one (T5u60), referred hereafter as the "free-field" station, is installed in the parking area at a distance of approximately 50m from the Northern façade of the structure. Both stations are oriented along the N-S direction (almost aligned with the x-x direction of the building, shown in Fig. 10) and operate on a continuous-recording mode at 100 sps, allowing for simultaneous recordings of seismic motion at the foundation level and free-field conditions.

A set of ten earthquakes (EQ) that occurred during the period of 14/02/2012 to 26/01/2014 with available recordings from both the foundation and the free-field station is presented herein. Basic earthquake metadata for the above earthquakes, retrieved from the Seismological Station of Aristotle University of Thessaloniki (http://geophysics.geo.auth.gr/ss/), are summarized in Table 1, where R refers to the distance between each earthquake epicenter and the COSMOS site. A representative pair of recordings produced by EQ.1 is plotted in Fig. 12 indicating the filtering effect of the foundation in the time domain. It is noted that a maximum peak ground acceleration of 6mg was recorded by the free-field station following the EQ.5 earthquake, indicating the low amplitude motion imposed on the soil-structure system for the specific set of records. As a result, the above range of PGAs allows for the implementation of the low-strain shear velocity mentioned above.

Given the low amplitude of the recorded motions, signal-to-noise ratios were computed for each record in order to estimate a reliable, noise-free frequency range for the transfer function between foundation and free-field motion. The above preliminary investigation revealed that up to 15 Hz the signal-to-noise ratio retains values larger than 3, that may be considered as an acceptable lower bound. The foundation-to-free-field Fourier amplitude ratio ($U_{\text{fnd}}/U_{\text{ff}}$) was then derived for each earthquake and the mean transfer function averaged over the ten Fourier ratios is shown in Fig. 13. So far, no data smoothing was performed, which explains the large frequency spikes observed in Fig. 13, since the main objective of the research at this stage

was to highlight a general trend of the kinematic-induced effects on the foundation motion. A more rigorous approach would require deriving smoothed transfer functions based on power spectral density functions rather than Fourier spectra to estimate the coherence between input (free-field) and output (foundation) motion, based on time or frequency domain methods that have been reported in the literature [21]. For this reason the data reported in Fig. 13 may be employed for a qualitative comparison between the earthquake records and the prediction of the proposed analytical model that follows.

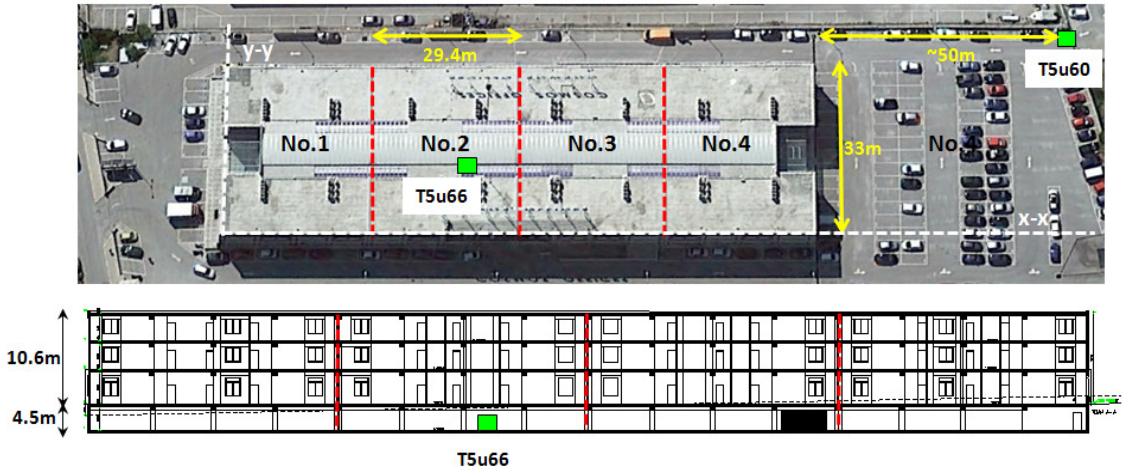

Figure 10: Google Earth Image of the COSMOS Offices building complex (top), composed of four identical buildings separated by seismic joints (shown with red dotted lines) and cross section of the building along the longitudinal direction (bottom). The location of the two accelerometric stations installed at the basement (T5u66) and the parking area (T5u60) of the building are also shown.

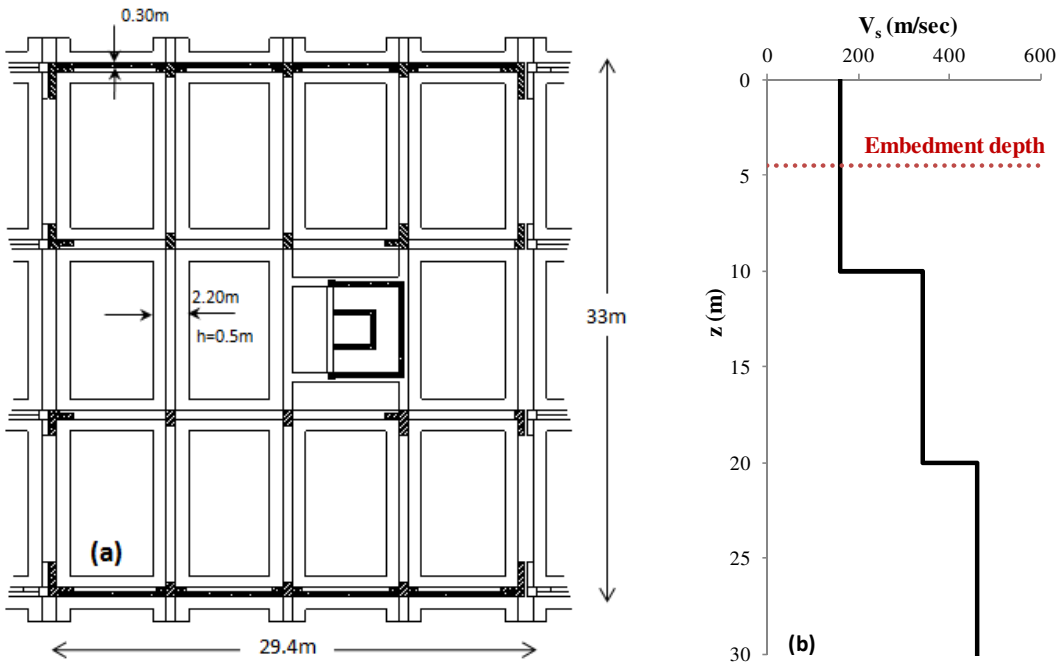

Figure 11: (a) Plan view of a typical building's foundation of the COSMOS Offices premises; (b) Shear wave velocity profile until the depth of 30 m measured by the MAM method at a distance of approximately 600m away from the structure [20].

Earthquakes	Day / Month / Year	Hr : Mn : Sc	M	Latitude	Longitude	R (km)
EQ.1	09 / 12 / 2012	**03:22:23.3**	**3.0**	40.644	23.034	10.51
EQ.2	12 / 05 / 2012	**22:48:12.8**	**3.9**	40.564	22.841	12.58
EQ.3	02 / 07 / 2013	**10:45:22.1**	**4.6**	40.118	21.853	108.05
EQ.4	03 / 07 / 2013	**13:28:23.8**	**4.6**	40.115	21.846	108.73
EQ.5	11 / 10 / 2013	**05:15:46.9**	**4.4**	40.690	23.410	38.64
EQ.6	26 / 01 / 2014	**13:55:41**	**5.9**	38.154	20.287	354.3
EQ.7	11 / 08 / 2013	**10:23:43**	**3.6**	40.230	23.104	36.3
EQ.8	08 / 09 / 2013	**10:33:00**	**3.5**	40.848	22.762	35.36
EQ.9	14 / 02 / 2012	**01:34:38**	**5.0**	40.129	24.089	104.6
EQ.10	21 / 10 / 2012	**04:43:31**	**3.4**	40.695	23.301	27.4

Table 1: Seismological metadata of the earthquakes recorded by the two accelerometric stations in the COSMOS Offices building complex (Data retrieved from seismicity catalogues reported by the Seismological Station of Aristotle University of Thessaloniki, http://geophysics.geo.auth.gr/ss/)

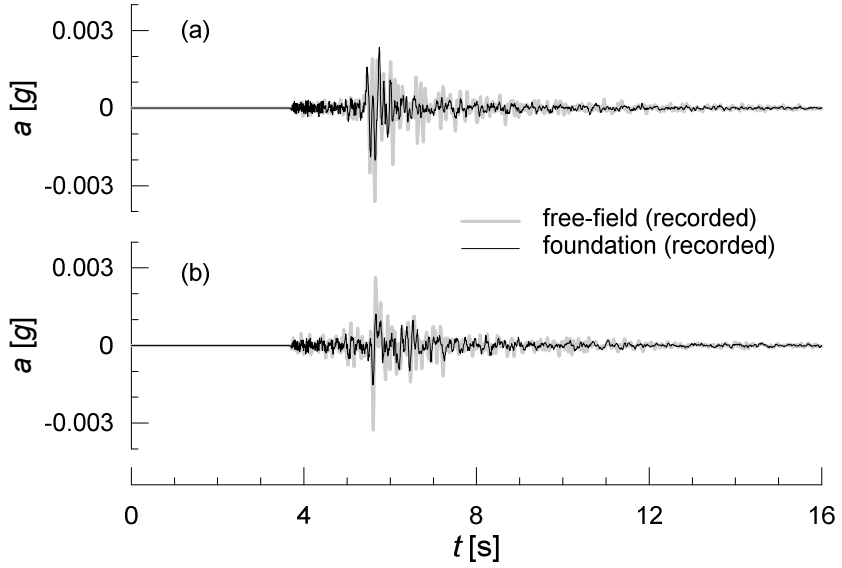

Figure 12: Earthquake EQ.1: foundation and free-field recordings: (a) E-W component (b) N-S component

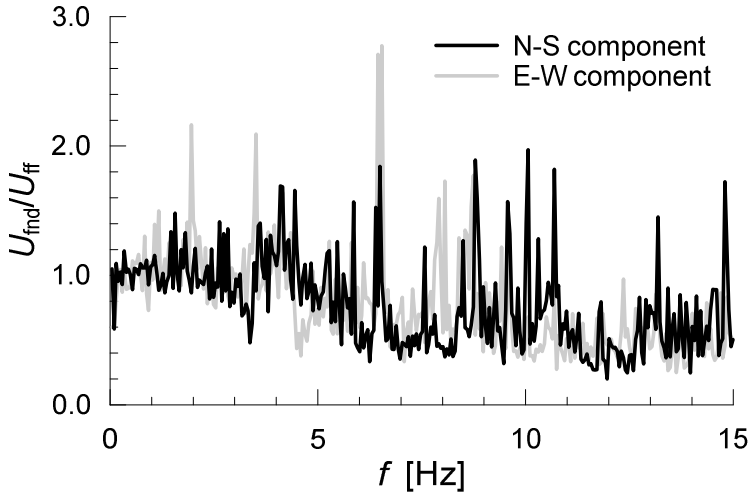

Figure 13: Unsmoothed foundation-to-free-field transfer function averaged over the Fourier ratios of the ten available pairs of recordings for both NS and EW component.

5.3 Interpretation of COSMOS building earthquake recordings

In order to highlight the role of the foundation mass in filtering the free-field motion, the available recordings were first interpreted using the approximate function of $|I_u|$ (Eq. 12) referring to both the massless (pure kinematic interaction) and the massive (quasi-kinematic interaction) case. Moreover, after modeling the COSMOS building as an equivalent SDOF system, the complete SSI problem was investigated by means of the classical Substructure method [4]. To this end, two different approaches were implemented: (i) a *standard substructure approach*, according to which the FIM motion is computed from a pure kinematic interaction and then the inertial interaction problem is addressed taking into account the mass of both the structure and the foundation; and (ii) a *hybrid substructure approach*, according to which the FIM motion is derived from a quasi-kinematic interaction and then the inertial interaction problem is solved including the sole mass of the structure. In both approaches, the expressions provided by Pais & Kausel [22] were used to compute the dynamic impedances for the embedded foundation.

The soil deposit is modelled as a uniform soil layer with mass density $\rho_S = 1.8$ t/m^3, constant shear wave velocity $V_S = 160$ m/s, Poisson's ratio $\nu_S = 0.3$ and damping ratio $\xi_S = 5$ %.

Based on the modal analysis of the MDOF lumped mass model for the COSMOS building, the equivalent fixed-base SDOF system is characterized by a height $H_{str} = 8.73$ m, a structural mass $m_{str} = 895$ t, a damping ratio $\xi = 5$ % and a natural period of $T_{0,N\text{-}S} = 0.47$ s and $T_{0,E\text{-}W} = 0.40$ s, along the N-S and E-W direction respectively.

As far as the foundation model is concerned, the plan dimensions are 29.4 m and 33.0 m, along the N-S and the E-W direction respectively, while the embedment depth is $H = 4.8$ m. The total mass of the foundation is $m_F = 4134$ t, leading to an equivalent mass density of $\rho_F = 0.9$ t/m^3 and a density ratio of $\rho_F/\rho_S = 0.5$.

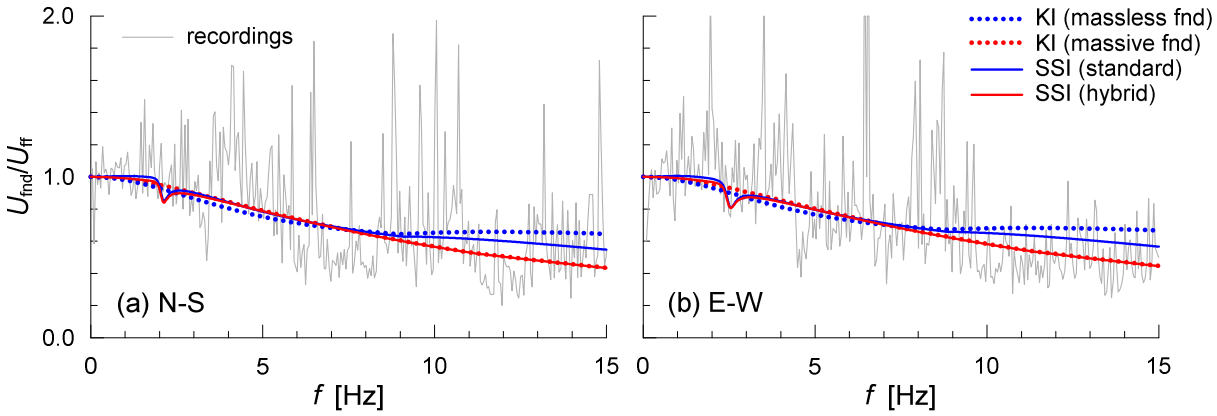

Figure 14: Comparison of recorded (unsmoothed) foundation-to-free-field transfer functions with theoretical predictions of the Substructure method applied to Cosmos Building along the: (a) N-S and (b) E-W direction.

Figure 14 shows the main results obtained by applying the Substructure approach to the COSMOS building, in terms of the foundation-to-free-field motion (U_{fnd}/U_{ff}), compared with the available foundation-to-free-field transfer functions along the (a) N-S and (b) E-W direction. Dotted lines refer to the kinematic interaction factor $|I_u|$, (Eq. 12), while continuous lines refer to the foundation motion resulting from the complete dynamic SSI, thus taking into account both kinematic and inertial effects. The trend observed in the two directions is very similar. Specifically, inertial effects stemming from the oscillation of the superstructure are observed within a narrow range around the fixed-base fundamental frequency of the SDOF. Thus, the reduction of the foundation motion with respect to free-field is mainly due to the

interaction between the foundation and the soil. On the other hand, the $|I_u|$ functions for a massless ($\rho_F/\rho_S = 0$) and massive ($\rho_F/\rho_S = 0.5$) foundation are almost coincident up to about 8 Hz, thus indicating that, in this frequency range, the soil-foundation interaction is purely kinematic, the foundation mass having indeed a negligible effect. However, the foundation mass does affect the foundation motion at larger frequencies, where the quasi-kinematic predictions provide a better comparison with the available recordings.

6 CONCLUSIONS

- This paper addressed the issue of the filtering effects induced by rigid massive embedded foundations subjected to vertically propagating shear waves. Based on the results from dimensional analysis and numerical FDM simulations, it was found that the problem can be described by three sole dimensionless parameters, namely: (i) $\omega H/V_S$, relating the wave length of the signal to the embedment depth H of the foundation; (ii) the aspect ratio of the foundation, B/H, where B is a characteristic length of the foundation width in the polarization plane; and (iii) the mass density ratio ρ_F/ρ_S between the foundation and the soil.
- Numerical analyses showed that the foundation mass can play a significant role on the kinematic interaction factors $|I_u|$ and $|I_{u,top}|$, while having a minor effect on the rotational component of the foundation motion, as reflected by $|I_\theta|$.
- Based on numerical results and theoretical 1D models, new simplified and physically sound expressions were derived for the kinematic interaction factors, $|I_u|$, $|I_\theta|$ and $|I_{u,top}|$.
- The proposed functions have been applied to the interpretation of the earthquake recordings available for the COSMOS Offices building in Greece. The comparison has confirmed the previous theoretical findings and has shown how to identify the contribution of the foundation mass in filtering the free-field motion, by means of a simple quasi-kinematic interaction analysis.
- The proposed functions can be applied both to the seismic design of structures with embedded foundations and to the interpretation of available recordings.

REFERENCES

[1] J. Bielak, Dynamic behavior of structures with embedded foundations. *Earthquake. Engng. Struct. Dyn.*, **3**, 259-274, 1975.

[2] A.S. Veletsos, A.M. Prasad, W.H. Wu, Transfer functions for rigid rectangular foundations. *Earthquake. Engng. Struct. Dyn.*, **26**, 5-17, 1997.

[3] F. Elsabee, J.P. Morray, Dynamic behavior of embedded foundation. Rep. No. R77-33, Dept. of Civil Engineering, Massachusetts Institute of Technology, Cambridge, Mass, 1977.

[4] G. Mylonakis, S. Nikolaou, G. Gazetas, Footings under seismic loading: Analysis and design issues with emphasis on bridge foundations. *Soil Dyn. Earthquake Eng.*, **26**(9), 824-853, 2006.

[5] J. Avilés, M. Suarez, F.J. Sanchez-Sesma, Effects of wave passage on the relevant dynamic properties of structures with flexible foundation. *Earthquake. Engng. Struct. Dyn.*, **31**, 139-159, 2002.

[6] R. Di Laora, L. de Sanctis, Piles-induced filtering effect on the Foundation Input Motion. *Soil Dyn. Earthquake Eng.*, **46**, 52-63, 2013.

[7] M. Mahsuli, M.A. Ghannad, The effect of foundation embedment on inelastic response of structures. *Earthquake. Engng. Struct. Dyn.*, **38**(4), 423-37, 2009.

[8] A.S. Veletsos, J.W. Meek, Dynamic behavior of building-foundation systems. *Int. J. Earthquake Eng. Struct. Dyn.*, 3(2), 121-38, 1974.

[9] D.L. Karabalis, Non-singular time domain BEM with applications to 3D inertial soil–structure interaction. *Soil Dyn. Earthquake Eng.*, **24**, 281-293, 2004.

[10] J. Liang, J. Fu, M.I. Todorovska, M.D. Trifunac, Effects of the site dynamic characteristics on soil–structure interaction (I): Incident SH-Waves. *Soil Dyn. Earthquake Eng.*, **44**, 27-37, 2013.

[11] J.M. Mayoral, M.P. Romo, Seismic response of bridges with massive foundations. *Soil Dyn. Earthquake Eng.*, **71**, 88-99, 2015.

[12] R. Conti, M. Morigi, G.M.B. Viggiani, Filtering effect induced by rigid massless embedded foundations. *Bull Earthquake Eng.*, **15**(3), 1019-1035, 2017.

[13] S.M. Day, Seismic response of embedded foundations. Proc. ASCE Convention, Chicago, IL, October, Preprint No. 3450, 1978.

[14] J. Dominguez, Response of embedded foundations to travelling waves. Report R78-24, Dept. of Civ. Engrg., Mass. Inst, of Tech., Cambridge, Mass, 1978.

[15] D.L. Karabalis, D.E. Beskos, Dynamic response of 3-D embedded foundations by the boundary element method. *Comput. Methods Appl. Mech. Eng.*, **56**, 91-119, 1986.

[16] J.E. Luco, H.L. Wong, Seismic response of foundations embedded in a layered halfspace. *Earthquake. Engng. Struct. Dyn.*, **15**, 233-247, 1987.

[17] A. Mita, J.E. Luco, Impedance functions and input motions for embedded square foundations. *Journal of Geotechnical Engineering*, ASCE, **115**, 491-503, 1989.

[18] Itasca, *FLAC Fast Lagrangian Analysis of Continua v.7.0. User's Manual*, 2011.

[19] Computers and Structures Inc., "*SAP 2000 - Structural Analysis Program: Linear and Nonlinear Static and Dynamic Analysis and Design of Three-Dimensional Structures*", Berkeley, California, USA, 2004.

[20] M. Manakou, P. Apostolidis, D. Raptakis, K. Pitilakis, Determination of soil structure in the broader urban Thessaloniki area. Proc. 3rd Hellenic Conference of Earthquake Engineering and Engineering Seismology, Athens, Greece, paper No 1978, 2008 (in Greek).

[21] A. Mikami, J.P. Stewart, M. Kamiyama, Effects of time series analysis protocols on transfer functions calculated from earthquake recordings, *Soil Dyn. Earthquake Eng.*, **28**, 695-706, 2008.

[22] A. Pais, E. Kausel, Approximate formulas for dynamic stiffnesses of rigid foundations. *Soil Dyn. Earthquake Eng.*, **7**(4), 213-227, 1988.